

Link Quality Evaluation of a Wireless Sensor Network in Metal Marine Environments

David Rojas · John Barrett

Received: 28/08/2017 / Accepted: 07/04/2018

Abstract Wireless sensor networks (WSN) are finding increasing use in all-metal marine environments such as ships, oil and gas rigs, freight container terminals, and marine energy platforms. However, wireless propagation in an all-metal environment with ducting and sealed doors between compartments is difficult to model, and the operating machinery further complicates wireless network planning. This makes it necessary to characterize the performance of the physical wireless links in the actual operating environments. However, little has been reported in the literature on methodologies for measuring the full range of physical link quality indicators. In this paper, we present a methodology for doing this that we have verified by the deployment of a 2.4 GHz network of 18 nodes in three different all-metal scenarios: a cluster of freight containers, a full-sized shore-based working ship's engine room training facility, and an operational ship's engine room. The output variables included the key link quality indicators of packet delivery ratio (PDR), RSSI, and LQI for every possible link, as well as the performance of every node. We believe that this is the first

time that this full range of physical link quality indicators has been measured in this type of application environment. We found that in all three scenarios the network performed with over 90% PDR average. However, as the scenarios become more complex, the communications become more unpredictable, yielding a wider transition zone, indicating that although a WSN could operate in these scenarios under different conditions, a pre-deployment practical study is essential for each new scenario.

Keywords Wireless Sensor Networks · Link Quality · Marine Metal Environments.

1 Introduction

Wireless sensor networks (WSN) can be used as a low cost alternative to wired sensors for optimizing the operation, efficiency, and maintenance of all-metal marine environments such as ships, oil and gas rigs, freight container terminals, and marine energy platforms. However, the large amounts of metal and complex layouts make it very challenging to model the wireless propagation in these all-metal environments. Ducts, pipes and sealed bulkhead doors between compartments further complicate wireless planning. Marine machinery in these environments will also affect communications, particularly with the high volume-occupancy of machinery in ships' engine rooms. To specify wireless network architectures and protocols, and to design applications for these metallic offshore environments, it is essential to measure the link quality in situ, as it cannot be accurately modeled and predicted [3, 25, 34]. Although power consumption is also a common issue in WSN, data reliability becomes the most important challenge in metallic environments, as multi-path can cause packet data loss and node placement decision becomes difficult. Therefore, the objective is to develop a systematic methodology to be used in these com-

This material is based upon works supported by the Science Foundation Ireland under Grant No. 12/RC/2302, the Marine Renewable Energy Ireland (MaREI) Centre research programme. This is a post-peer-review, pre-copyedit version of an article published in Springer Wireless Networks. The final authenticated version is available online at: <http://dx.doi.org/10.1007/s11276-018-1726-z>

David Rojas · John Barrett (✉)
Nimbus Centre, Cork Institute of Technology
Bishopstown
Cork
Ireland
E-mail: f.rojas-calvente@mycit.ie

David Rojas
E-mail: f.rojas-calvente@mycit.ie

John Barrett
E-mail: john.barret@cit.ie

plex metallic scenarios, which can provide an accurate view of the communication performance of a WSN in these environments. Thus, data reliability can be guaranteed by an optimal node deployment and the use of dependable protocols.

In this paper, we first present the analysis performed in [22], where we deployed a network of 18 IEEE 802.15.4-compatible nodes transmitting at 2.4 GHz in three freight containers, and we expand it with a series of experiments in two more complex scenarios: a shore-based, full-sized, operational ship's engine room training facility and a seagoing Irish Naval Service ship's engine room. We present a comprehensive methodology for fully characterizing link quality at the physical level in metallic complex environments and the verification of the methodology in the three scenarios. In the methodology, we varied input variables that could influence link quality and we recorded output variables which were the key link quality metrics. In contrast with previous reported works done in similar environments, we focus on physical link quality instead of application-level or network-level topology; we also characterized the effect of operational machinery on the output variables.

The results allowed us to classify links reliability, asymmetry, and sink candidates, and to analyze the behaviour of the network at a high level of detail. This information would be required in practice for the planning and design of higher-layer protocols and applications, and ultimately the deployment and management of robust WSN applications.

The remainder of the paper is structured as follows: Section 2 discusses related work and sets out the novelty and work in this paper. Section 3 presents the experiment designs, variables, hardware and software for the three node deployment scenarios. Section 4, 5 and 6, contain the specific experiments and description for each of the three scenarios respectively (freight containers, shore-based engine room and ship's engine room), including a detailed analysis of the results. Section 7 presents the conclusions.

2 Related work

WSN applications have been successfully deployed in a wide range of indoor and outdoor scenarios. WSN technology also underpins the Internet of Things. They all have in common the use of battery-powered wireless resource-constrained nodes with a variety of low-power sensors from environmental to MEMs microphone and accelerometers. Indoor deployments include office buildings [27], to monitor occupancy and environmental variables and provide data intelligence to the HVAC systems for energy saving, which is also applied in a similar way to data centers [16]. Healthcare systems are also benefiting from WSN technologies, to improve current monitoring services specially for the elderly and children [1]. Outdoor scenarios have as well seen

an increasing number of WSN deployments in recent years: urban environments [20], agriculture [31], marine [29], machine and structural health monitoring [2], etc. WSN have also attracted industry [17], with the potential of lowering sensor cost and facilitating deployment. Industry scenarios however have some added challenges that are also common in offshore marine deployments: large amounts of metal and possible electromagnetic interference from heavy machinery.

Regarding metal environments, some experiments have been reported for monitoring shipping containers with WSN. In [30], a network was deployed on the outside of containers for location tracking, analysing application parameters such as the dynamics of routing, power consumption, and network topology, but not the link quality. Yuan et al.[32] tested a sensor network inside food cargo containers, recording the RSSI and link quality indicator (LQI) as well as the sensor data. However, their focus was primarily on the signal strength over distance, and the experiment was done with multi-hop and duty-cycling protocols.

Similar analyses have been carried out for WSNs on board ships as a cheaper alternative to wired networks, e.g., [13, 14]. These studies, using both simulations and practical measurements, show that communications between adjacent rooms and decks are possible due to signal leakage through bulkhead seals between compartments. In [11, 12], tests included more realistic shipboard variables, such as door opening and closing, operating machinery, and people movements. However, all of these were built on top of the XMesh and Zigbee protocols, focusing on the network topology and not on the analysis of physical links. Packet delivery ratio (PDR) and RSSI were measured but, due to the use of upper-layer protocols that involve retransmissions and mesh network configuration, they do not provide a comprehensive understanding of the propagation environment.

A key variable that affects WSN communications quality in marine environments, such as ships engine rooms and marine energy platforms, is electromagnetic interference (EMI) from electro-mechanical machinery. Despite the literature showing some assessments of broadband and out-of-channel interference in IEEE 802.15.4 networks [4, 7] and some preliminary simulations in ship environments [18], no experiments have been reported in a ship's engine room scenario with on/off switching of the machinery.

Rehmani *et. al* [21] performed experiments with TelosB nodes in two environments that can be considered the upper and lower bound of multi-path effects, i.e., reverberation chamber and anechoic chamber. Although focusing on antenna diversity, the results of these experiments provide some insight into the expected effects in real metallic multi-path environments. While the anechoic chamber showed more stability in the RSSI values, the results in the reverberation chamber indicated a much higher temporal vari-

ation for the RSSI in the same node (a maximum of 9 dB) as well as in the PDR of different nodes that were just 5 cm apart.

Although the literature shows several of these WSN deployments in different metal and ship environments, none of them use the methodology in this paper, which allows an analysis of the link quality between the nodes in an “all-to-all” fashion with probe synchronisation and a systematic assessment of effects of the different variables. This allows more accurate characterization that includes the effects of realistic WSN deployment variables such as node position and orientation, openings between adjacent compartments, node transmission power, and EMI.

3 Experiment setup

3.1 Testbed environments

We carried out the experiments in three different scenarios with increasing complexity and scale. The first deployment, in three outdoor freight containers, assessed the effect of door openings, node location and orientation on the communications. The second was in a shore-based full-sized ship’s engine room training facility (in this paper we refer to this as the “engine room emulator”). This contained a large amount of piping and metal fixtures, as well as several electrical generators and a ship’s engine that could be individually and collectively switched on and off to test the effect of electrical noise. The third deployment was on a seagoing Irish Naval Service (INS) ship’s engine room and its adjacent compartments, where we varied the opening of the sealed bulkhead door as well as the switching of the main engine and generators. To characterize link behaviour, we designed a full factorial experiment in which we varied one variable at a time. We designed each experiment to be completed in a single day with a randomized run order to minimize the confounding effects of the environmental variables of humidity and temperature. These scenarios and experiment designs are described in more detail below in their respective sections.

3.2 Hardware and software tools

The hardware for all three deployments consisted of 18 TelosB nodes [19], plus an extra gateway node connected to a laptop to configure the experiment and download the data. The nodes comprised a low-power microcontroller, a 2.4 GHz IEEE 802.15.4 radio chip, an on-board PCB antenna, and several integrated environmental sensors. We chose these nodes for their wide use in research and good software support.

To conduct the tests, we used an open-source software tool TRIDENT [10] which, unlike similar tools available,



Fig. 1 Outside view of the freight container testbed.

allowed us to configure and run the experiments without the need for a separate wired infrastructure. This makes it easier to change node locations between different runs and to retrieve the data via multi-hop wireless communication. The tool allows configuration of every node as a sender and receiver, synchronising the senders in a round-robin fashion to avoid collisions and ensuring that there will not be more than one node transmitting at the same time. This feature, along with the ability to send probes without any MAC or upper-layer protocols, is key to accurate characterization of the physical medium. The nodes acting as receivers log the number of received packets, RSSI and LQI, besides the noise floor sensed by the sender before transmission, and environmental variables. The measured LQI can be seen as an approximation of the chip error rate; it is dimensionless and measures the strength quality by calculating the average correlation of the first eight symbols of the received packet, with values ranging from 110 (best quality) to 50 (worst). This tool has been previously successfully used in different open field deployments, e.g., [6, 15].

4 Scenario I: Freight containers

4.1 Environment description & experiment design

The nodes were installed inside and outside three freight containers located in an outdoor yard and separated by 3 to 4 m, with various metal and concrete obstacles between them (Fig. 1). Containers 1 and 2 are 6 m x 3 m, while container 3 is slightly smaller at 6 m x 2.5 m. This constitutes a unique indoor/outdoor metal environment that more realistically replicates the real-world environments. The distribution of the containers and the nodes can be seen in Fig. 2. The containers contain several pieces of furniture such as tables and metal shelves, including a small metal box where node 9 is placed. It should be noted also that container 2 has a double door, a metal exterior door and a wooden interior

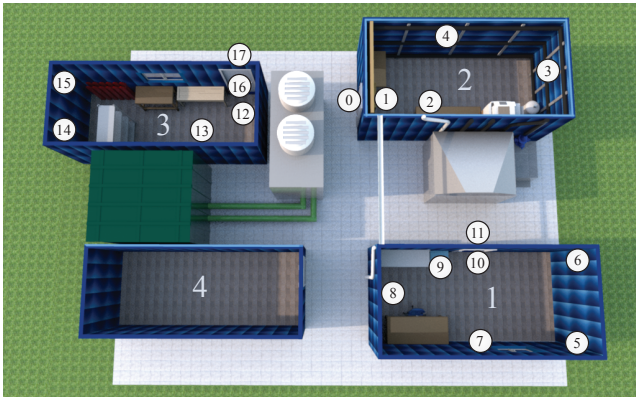


Fig. 2 Node distribution in the containers.

door, but these were opened and closed as one door and not considered as separate variables.

The set of variables and levels for this environment are in Table 1. An important issue in these multi-chamber environments is the size of the openings between adjacent rooms. Therefore, we selected three different door openings for the containers to emulate this: fully closed, a minimum opening of 5 cm (approximately a half-wave for the frequency used), and a maximum opening of 40 cm, which corresponds to the size of an opening, such as a bulkhead door, that would allow a person to pass through. As sensor nodes will typically be used to monitor different parts of the structure and machinery, their height, position, and orientation will vary. We therefore selected two heights: middle height (1.7 m), and ground level (0 m); and, because the antenna is not isotropic, we selected the best and worst case: node attached horizontally and vertically. Finally, as the software tool allows us to interleave every round of packets with different transmission power levels, we set two levels of 0 dBm (maximum power) and -5 dBm, which would suppose around 20% reduction in power consumption. Although energy consumption is not an issue that can be studied in these experiments, the results obtained will become important for future work when a real sensing application is deployed, which can include multi-hop and/or retransmissions. A more reliable link would need less hops and packet retransmissions to reach the sink, therefore consuming less energy. All combinations of these variables form a total of 24 experiments, organized in 12 different runs with two interleaved powers.

We placed the nodes inside containers 1 to 3, Fig. 2, to cover key points such as corners, doors, and problematic areas behind metal shelves or furniture. Container 4 could not be used due to restricted access. We attached three nodes (0, 11, and 17) to the outside of the doors, to allow connectivity through the doors' leakage. Since node 0 acts as the master node for synchronising and distributing the experiment to all the nodes, we choose its location to be at a midpoint distance from the rest and therefore the best candidate for

Table 1 Experiment variables.

Variable	Levels
Transmission power	0 dBm, -5 dBm
Node distance from ground	0 m, 1.7 m
Node antenna orientation	Horizontal, Vertical
Container door openings	Closed, Open 5 cm, Open 40 cm

the sink. This is not essential, as there are multi-hop capabilities for distributing the configuration, but nevertheless a good location of the master node can facilitate it.

We performed all experiment runs on November 24th 2015, on a clear winter day. For each run configuration, we sent four rounds of probes per node, 2 at high and 2 at low power, with each round composed of 10 probes with a 750 ms gap between them, and each probe with a burst of 10 messages with 50 ms separation. This forms a total of 200 messages per round and power level per node. We made the decision to perform burst experiments based on the target application, considering that machine and structural monitoring often require data bursts from accelerometers and other high sample rate sensors [23]. The probes used channel 26, to avoid interference with Wi-Fi networks, and were configured not to use any MAC protocol. Each run configuration lasted for 10-15 min, accounting for the probe sending and the data writing to the memory which, along with changing the position of the nodes and data downloading, used the full day of experiments for the total set of 12 runs.

4.2 Results & analysis

4.2.1 Overall network analysis

A simple way to get a general understanding of the link quality of a wireless network is by looking at the RSSI, and its relationship with the PDR and LQI [3]. Although the presence of interfering signals can boost the RSSI levels while yielding a lower PDR [33], the setup of our experiments guarantees a lower chance of that occurring, due to channel selection and environment isolation.

In Fig. 3, we represent the PDR of each probe burst for the different combinations of rounds, for high (0 dBm) and low (-5 dBm) power, with respect to the mean RSSI. A total of $n(n-1) = 306$ links, with $n = 18$ nodes, were analyzed for each round. We observe the typical overturned "L" shape found in the literature [24, 26], with disconnected, transitional, and connected areas. This can also be seen in Fig. 4, which shows how LQI relates to RSSI. However, we can see some outliers (circled) in both plots occurring in node 11, which is attached to the outside of the door in container

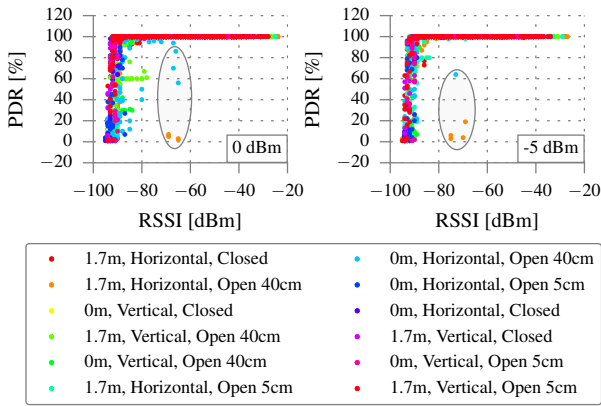


Fig. 3 PDR vs RSSI.

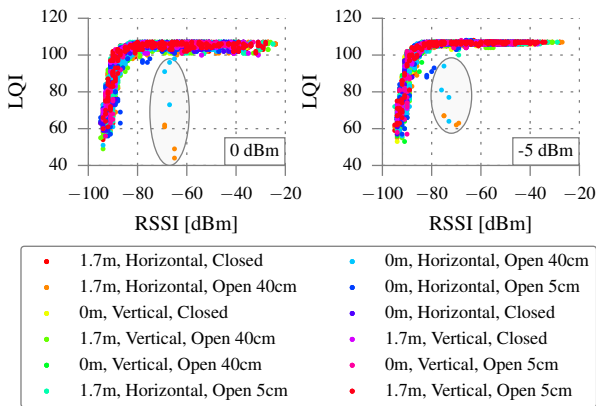
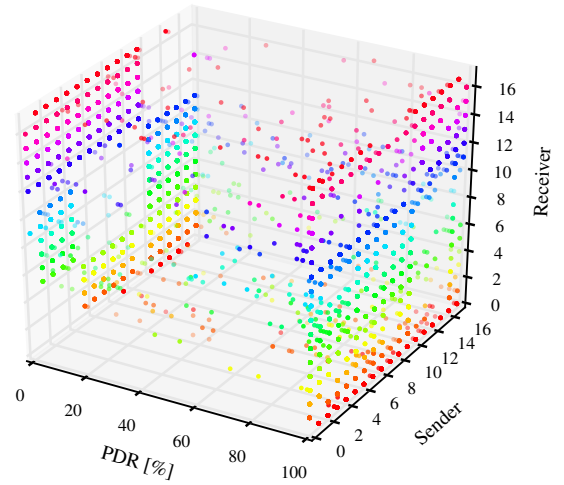


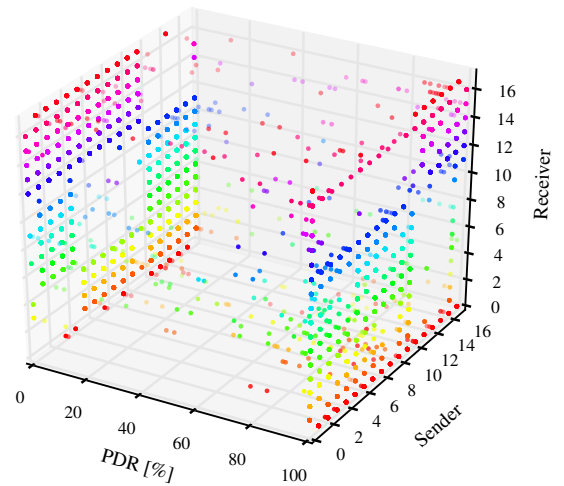
Fig. 4 LQI vs RSSI.

1, for the configurations with the doors open. Since external interference is unlikely, we speculate that this could be due to the multipath caused by the amount of metal in the environment. Moreover, the overall noise floor measured is fairly constant and close to the sensitivity of the radio chip, with an average of -96 dBm and $\sigma = 1.28$, which excludes the presence of other external elements that could affect the signal integrity.

To give a global view of the performance of each node, we show in Fig. 5 a 3D representation of the PDR per probe, accounting for each node being a sender or receiver. The first thing to notice is the high concentration of points near the 100% PDR plane, except for an empty rectangle between nodes 12-15 and 17, corresponding to the ones located in container 3, and with a concentration of points in a mirrored space on the 0% PDR plane. This could be due to two reasons: the door of this container faced away from the other two containers and the presence of the large metal block between container 2 and 3. This is more visible in the low power configuration. We can also observe the same empty block repeated, but rotated to the opposite side, suggesting a high degree of symmetry in the network. As asymmetry predicts the unreliability of a link, and has an impact on



(a) Transmission power at 0 dBm



(b) Transmission power at -5 dBm

Fig. 5 PDR [%] between each node for all rounds at different transmission powers.

upper-layer protocols [9], we decided to have a closer look at the average link asymmetry of individual nodes. In Fig. 6, we represent the asymmetry as defined in [26], where a link is considered asymmetric if $|PDR_{n \rightarrow m} - PDR_{m \rightarrow n}| > 40\%$. This shows that only links 11-13 and 15-17 exhibit a noticeable, although small, asymmetry ($< 10\%$), while most of the links are almost fully symmetrical.

4.2.2 Effects of the variables on network performance

We can see an interesting effect of the environment by looking at the average PDR and RSSI for each of the different door combinations, Table 2. Although we could see a positive correlation between PDR and RSSI when representing all bursts of probes in Fig. 3, the average values per com-

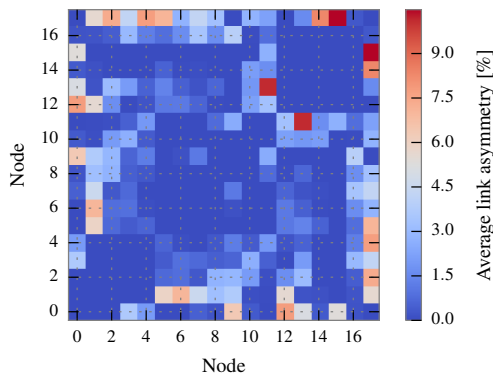


Fig. 6 Link asymmetry calculated as $|PDR_{n \rightarrow m} - PDR_{m \rightarrow n}|$.

bination shown in the table seem to indicate the opposite. This is due to the fact that, when any of the variables are set to have a negative effect on the signal range (e.g., closed doors), the average PDR computed over the whole network decreases; however, as the number of connected links also decreases, the average RSSI, which is calculated only over the remaining links, increases. This indicates that the network becomes more polarized, dropping links that were previously in the transitional region to the disconnected region. This effect can further be observed, for the individual variables, in the CDF representation of the PDR and RSSI in Fig. 7 and 8. In Tables 3 and 4 we can see that this is less noticeable for the node height and orientation variables, as they have less impact on the PDR.

We observe an increase of over 50% in the total PDR from closed doors to fully open at full power, while for the node height and orientation it is much less. Therefore, the number and size of the openings will be the key variables to take into account when deploying wireless networks in these environments.

As expected, the best performance occurs when the nodes are transmitting at high power, located at 1.7 m in horizontal, and with the container doors fully open, yielding an overall PDR = 74.69% and mean RSSI = -69 dBm. On the other hand, the worst case is found at low power, nodes vertically oriented at ground level, and doors closed, with a resulting PDR = 37.25% and mean RSSI = -66 dBm.

Due to the season and geographical area, the environmental variables recorded during the tests did not undergo dramatic changes, with an average temperature of 13.44 °C, $\sigma = 1.63$, and relative humidity of 68.03%, $\sigma = 12.76$, outside the ranges that can affect significantly the performance of the node wireless communications.

4.2.3 Link classification and sink selection

Although the 3D plots above allow quick identification of problem areas, we still need a way to quantify the link reliability to each specific node. For this we used the link classi-

Table 2 Average PDR and RSSI for different door openings.

Transmission power	Door state	PDR [%]	RSSI [dBm]
0 dBm	Closed	41.13	-64
	Open 5 cm	47.83	-67
	Open 40 cm	64.21	-70
-5 dBm	Closed	38.03	-66
	Open 5 cm	42.35	-68
	Open 40 cm	55.66	-71

Table 3 Average PDR and RSSI for different node heights.

Transmission power	Node height	PDR [%]	RSSI [dBm]
0 dBm	1.7 m	53.49	-67
	0 m	48.61	-68
-5 dBm	1.7 m	47.06	-68
	0 m	43.63	-69

Table 4 Average PDR and RSSI for different antenna orientations.

Transmission power	Orientation	PDR [%]	RSSI [dBm]
0 dBm	Horizontal	54.33	-67
	Vertical	47.78	-67
-5 dBm	Horizontal	48.17	-68
	Vertical	42.52	-69

fication described in [15, 26], which aggregates the links in five groups: *dead* ($PDR = 0\%$), *poor* ($PDR < 10\%$), *intermediate* ($10\% \leq PDR \leq 90\%$), *good* ($90\% < PDR < 100\%$), and *perfect* ($PDR = 100\%$). Fig. 9 shows the number of links to each node distributed in each category, from a total of 17 possible links per node, for high and low power configurations. This representation, along with the average total PDR per node shown in Fig. 10, allow identification of the node with the best quality links that would be a good candidate for a sink in a one-hop network.

We notice that, even though the average PDR drop from high to low power per node is not large, the number of dead links increases considerably. This renders most of the nodes incapable of acting as a sink, with the exception of nodes 0 and 11, located outside containers 1 and 2, which keep all their links in the connected and transitional region, due to their strategic location. Looking at Fig. 10, we can confirm that our initial placement of the master node (node 0) as a sink candidate was correct, as it yields a better performance than the rest of the nodes, with an average PDR = 91.97% for all round combinations of high power.

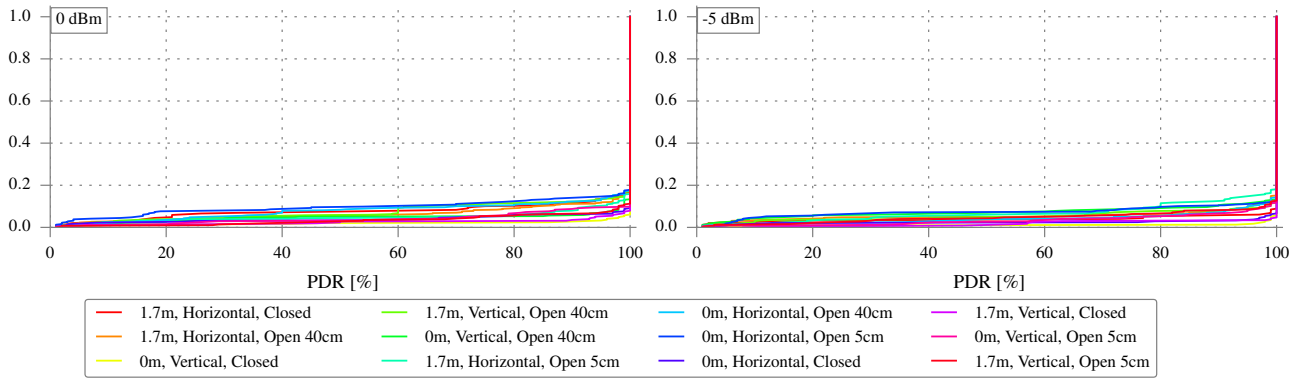


Fig. 7 CDF of the PDR.

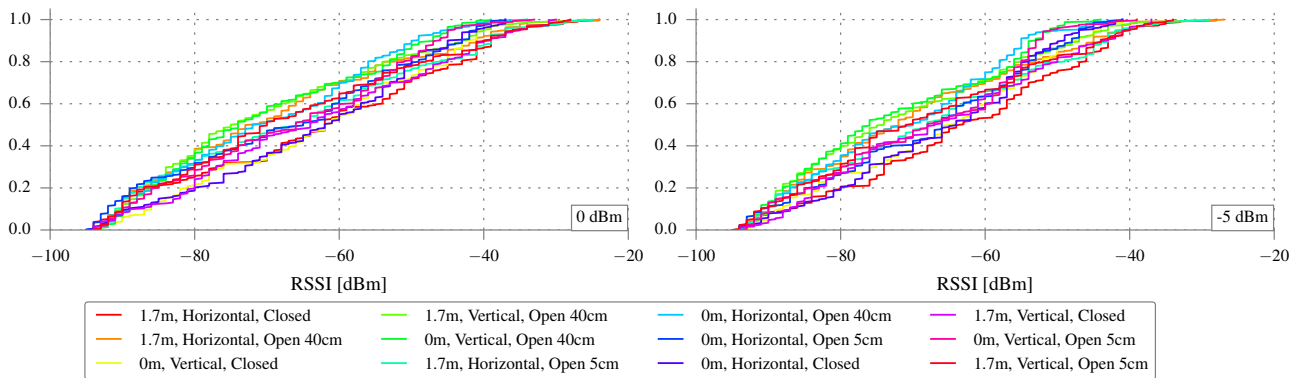


Fig. 8 CDF of the RSSI.

Since we established that the door openings are the most influential variable in our experiment, we show in Table 5 the average PDR and RSSI values for all the links to the sink candidate (node 0) for the different door configurations for both powers. In this case, unlike the previous case when we looked at the network links as a whole, we can see the expected increase in RSSI with the PDR, as a result of the links being stable under all different conditions. For the high power transmission, we observe a PDR = 80.65% for the closed door and a PDR = 98.33% for the open door case, with a 6 dB difference between both states, and a PDR = 96.92% is achieved with only a 5 cm door opening. Even at the worst case, with the doors closed and low power, we obtain an average PDR = 70.04% to the sink candidate.

5 Scenario II: Ship's engine room emulator

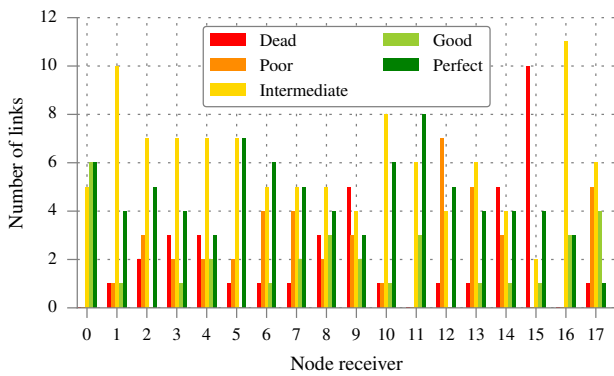
5.1 Environment description & experiment design

The previous scenario showed the behaviour of the network in a simple metal multi-chamber environment. To increase complexity, the next deployment was done in a full-scale operational engine room emulator, with control room, located in the National Maritime College of Ireland (NMCI), which

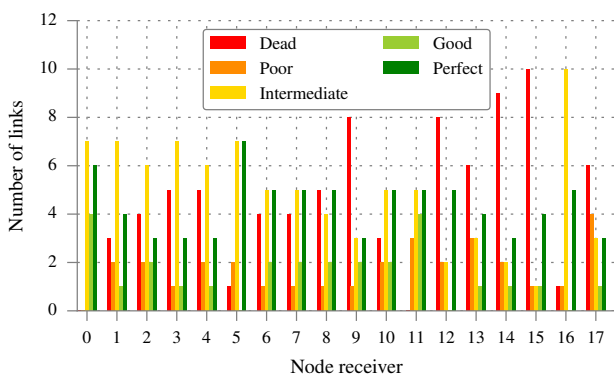
Table 5 Average PDR and RSSI for different door openings (node 0).

Transmission power	Door state	PDR [%]	RSSI [dBm]
0 dBm	Closed	80.65	-74
	Open 5 cm	96.92	-73
	Open 40 cm	98.33	-68
-5 dBm	Closed	70.04	-78
	Open 5 cm	88.69	-76
	Open 40 cm	97.77	-73

is normally used for marine engineering training. As we see in Fig. 11, this is a 16 m x 20 m high ceiling room full of various machinery, metal ducting and piping, gantries, etc., which are representative of the environment found not only in ships but in other off-shore structures. Moreover, from the control room in the center we can switch on/off a real ship's engine connected to a variable load, as well as an auxiliary generator. The ship engine is a MaK 60M20 running at 1000 RPM and the auxiliary generator a Caterpillar running at 1500 RPM. The 18 nodes were distributed to cover the whole room, as shown in Fig. 12. Nodes 2 and 4 were placed on top of the main engine, while node 3 was attached



(a) Transmission power at 0 dBm



(b) Transmission power at -5 dBm

Fig. 9 Number of *dead* ($PDR = 0\%$), *poor* ($PDR < 10\%$), *intermediate* ($10\% \leq PDR \leq 90\%$), *good* ($90\% < PDR < 100\%$), and *perfect* ($PDR = 100\%$) links for each node.

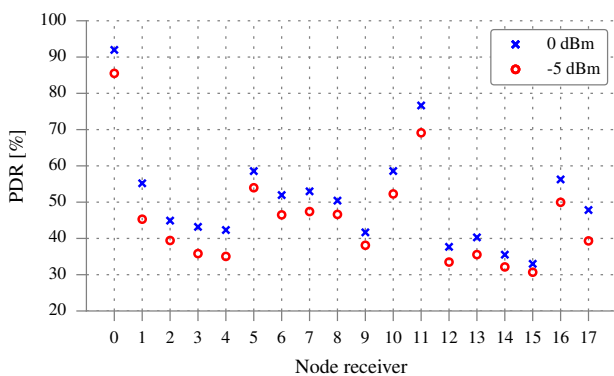


Fig. 10 Average total PDR [%] per individual node.

under the cover, and node 6 on top of the working auxiliary generator. We placed node 0 (master) at the most centered position, on the window sill outside the control room, at around 1.5 m from the ground.

In this scenario, we choose to vary the operation of the main engine and auxiliary generator to test the effect this might have on the network performance, as well as the transmission power (Table 6). Also, because the environment is



Fig. 11 Engine room emulator.

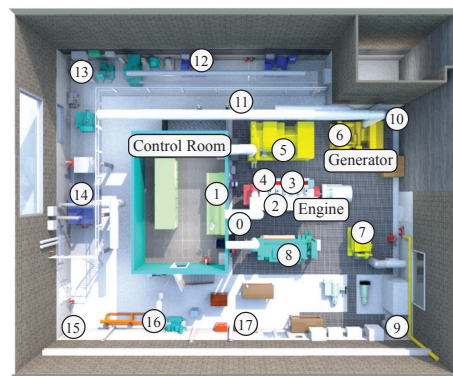


Fig. 12 Node distribution in the NMCI engine room.

Table 6 Experiment variables.

Variable	Levels
Transmission power	0 dBm, -5 dBm, -10 dBm
Machinery status	All off, Aux generator on, Aux generator + main engine on, All on + 200 KW load

an open space and can potentially yield a higher connectivity, we added an extra lower power level (-10 dBm) to the test rounds, to assess if we could further reduce transmission power to save energy.

The experiments were also completed in a single day, July 19th 2016, with the same configuration as in the previous one in terms of channel selected and messages per probe. However, because of the addition of the extra power level the number of rounds of probes per node was 6 (2 rounds per power).

5.2 Results & analysis

5.2.1 Overall network analysis

Fig. 13 and 14 show the PDR for each probe and average LQI with respect to the RSSI, respectively, for the three

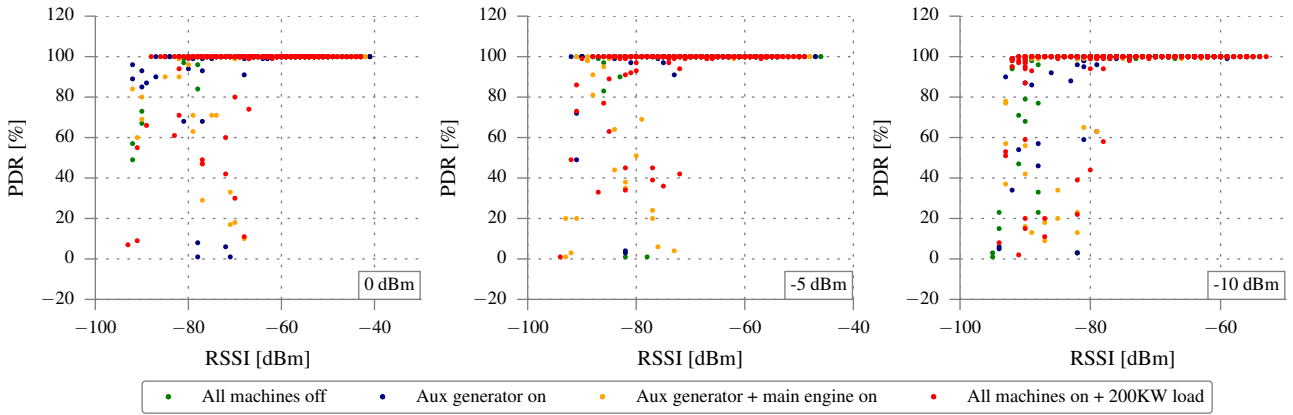


Fig. 13 PDR vs RSSI for the engine room emulator environment.

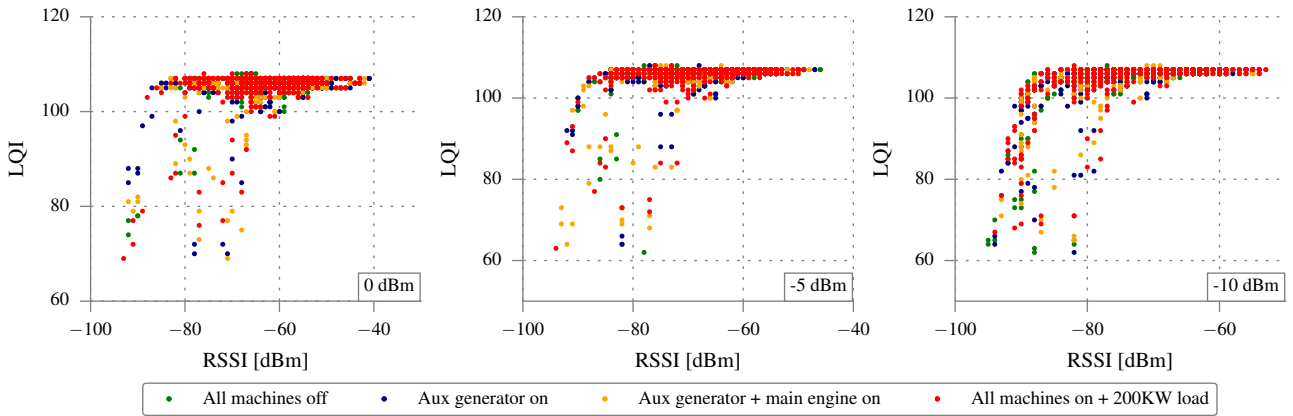


Fig. 14 LQI vs RSSI for the engine room emulator environment.

powers tested. Although we can still discern the L-shaped pattern and the different connectivity areas, we see more outliers compared to the previous environment, despite having a much shorter number of experiment runs. As the outliers are distributed among the different rounds, including the ones with machinery off, we can conclude that having the engine or generators on is not causing them. This increase could be produced, however, from the increase in the complexity of the environment i.e. the large amount of piping, machinery and metal surfaces present in the room, all of which can contribute to multipath. The noise floor stayed constant at -96 dBm, as in the previous scenario.

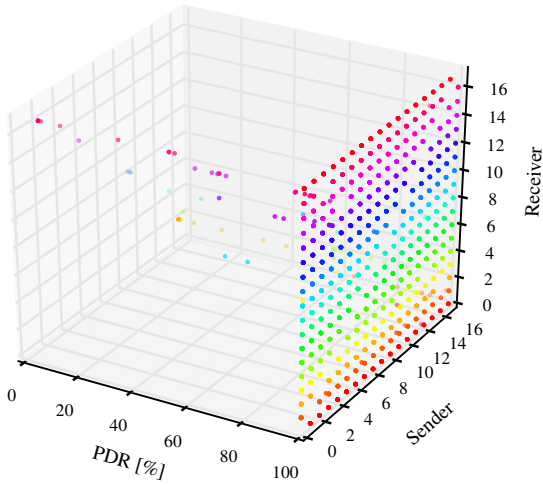
Due the environment being composed of a single relatively small open room, most of the probes were received with an average PDR close to 100% even for the low power configuration (-10 dBm), as we see in the 3D representation in Fig. 15, with the exception of nodes 14 and 4. The lowest PDR occurs in the link between them, consistent among all rounds. Although this may be due to the lack of line of sight between both nodes, node 3 should be exhibiting similar or worse behaviour, since it is located in the same place as node 4 but under the cover of the engine. However, node 3

performed better than node 4 overall, again suggesting that multipath can have unpredictable effects on the communications. If we look at the asymmetry representation of the links in Fig. 16, node 14 shows more than a 10% asymmetry in two of its links, which confirms this location as particularly unreliable.

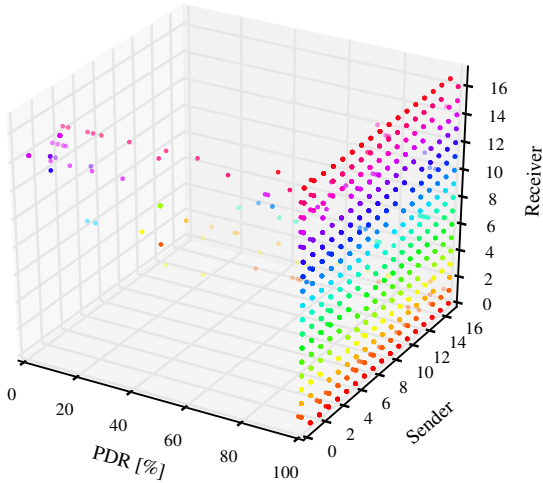
5.2.2 Effects of the variables on network performance

Table 7 shows the average PDR and RSSI obtained for the three powers tested for each machinery setting. The network on average showed a high connectivity for all the conditions, with over 97% PDR even for the worst case at -10 dBm; we can see the expected average 5 dB drop in RSSI with for every 5 dB reduction in transmitted power, indicating that the network maintained stable links with a only small decrease in PDR. This high connectivity can also be seen in the CDF representation of the PDR in Fig. 17, where the cumulative distributions are more concentrated in the 100% mark than in the previous scenario.

We can also observe a slight reduction in average PDR when we turn on different machines, although this could be



(a) Transmission power at 0 dBm



(b) Transmission power at -10 dBm

Fig. 15 PDR [%] between each node for all rounds at different transmission powers, for the engine room emulator environment.

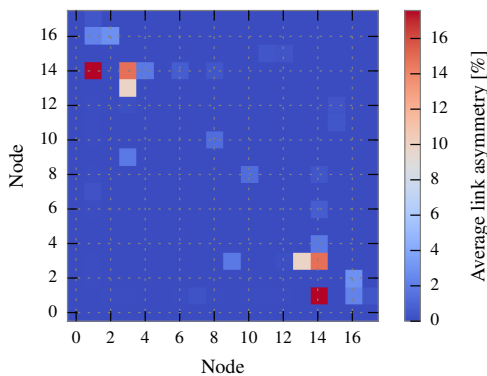


Fig. 16 Link asymmetry calculated as $|PDR_{n \rightarrow m} - PDR_{m \rightarrow n}|$, for the NMCI engine room.

Table 7 Average PDR and RSSI for different machinery states.

Transmission power	Machinery state	PDR [%]	RSSI [dBm]
0 dBm	All off	99.05	-62
	Aux generator on	99.12	-62
	Aux gen + engine on	98.85	-62
-5 dBm	All on + 200 KW	98.78	-62
	All off	98.65	-66
	Aux generator on	98.55	-67
-10 dBm	Aux gen + engine on	98.30	-67
	All on + 200 KW	98.31	-67
	All off	97.91	-72
-10 dBm	Aux generator on	97.94	-72
	Aux gen + engine on	97.07	-72
	All on + 200 KW	97.27	-73

due to the increase in temperature in the nodes located on top of the turned on devices instead of the electrical noise, which in some cases reached 40°C for the nodes on top of the main engine. The average temperature for all rounds was 25.16°C , stable for most of the nodes but with a $\sigma = 2.6$ due to the contribution to the average of those nodes. The CDF plot for PDR (Fig. 17) and RSSI (Fig. 18) also show this small increase, as the line representing the round with all machines on (red line) is above the others, indicating more accumulation of points in the lower PDR and RSSI respectively.

5.2.3 Link classification and sink selection

If we look at the number of links per node in each category, as previously defined for estimating link reliability, we see in Fig. 19 that all the nodes have most of their links with perfect connectivity for high power (0 dBm) and even for low power (-10 dBm). The exception is nodes 4 and 14, already identified as problematic, with the link between them dead for the low power configuration. Node 3 also presents a lower number of perfect links, due to the node being inside the enclosure of the main engine, although none of them dead or poor.

Fig. 20 shows that, when using a high power (0 dBm) configuration, all of the nodes present more than 95% PDR, therefore every node could act as a data sink if necessary. Avoiding node 14 would allow network reliability to be preserved, even at -10 dBm, saving power.

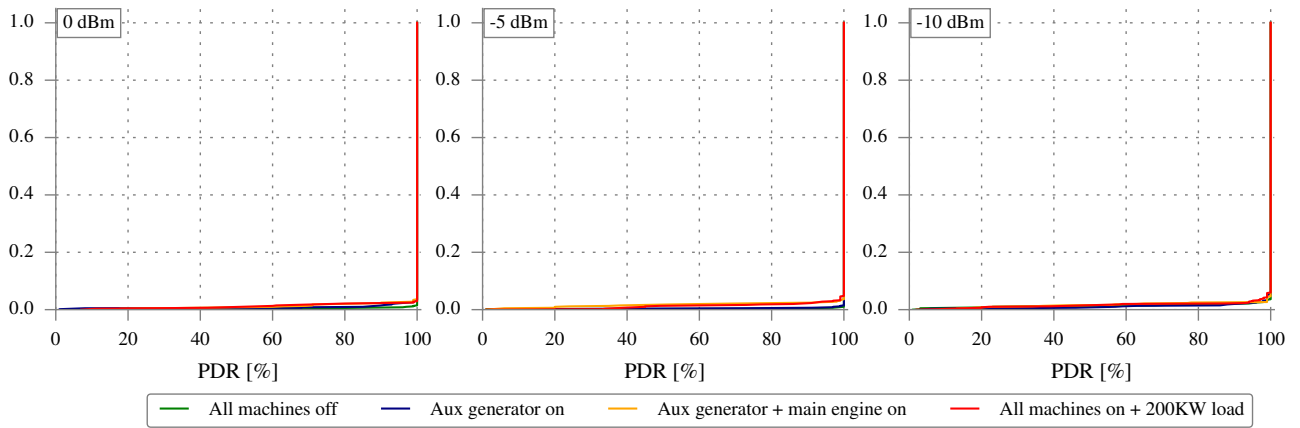


Fig. 17 CDF of the PDR for the engine room emulator environment.

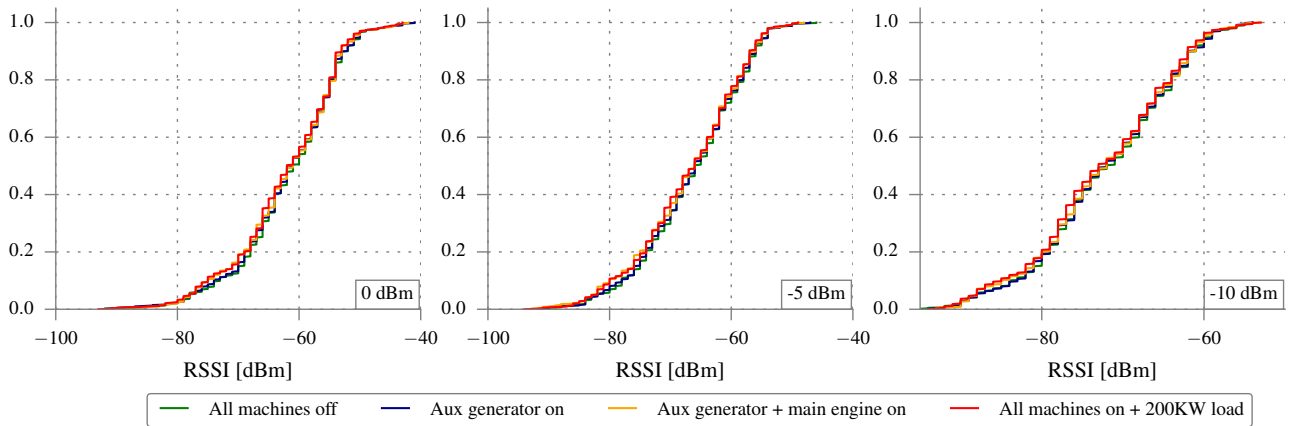


Fig. 18 CDF of the RSSI for the engine room emulator environment.

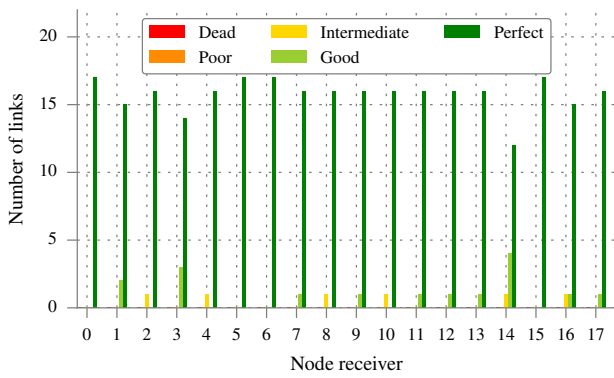
6 Scenario III: Naval vessel engine room

6.1 Environment description & experiment design

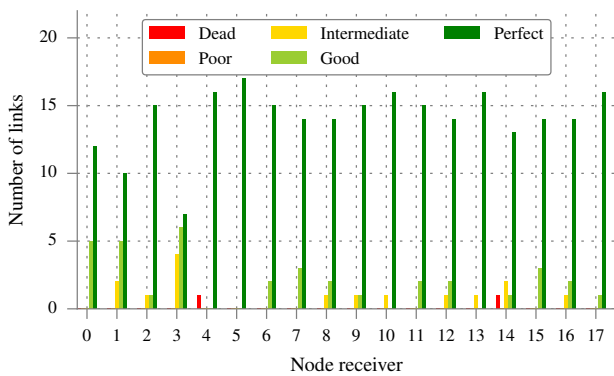
To perform a final set of experiments in a more realistic scenario, we deployed the same 18 nodes in the *LE Joyce* offshore patrol vessel of the Irish Naval Service (INS). We installed the nodes in the 10 m x 12 m engine room and its adjacent 9 m x 4 m compartment, connected by a waterproof sliding bulkhead door. Fig. 21 shows different views of the rooms, showing similar piping as in the NMCI emulator room but with overall higher volume occupancy of metal, with many more metal components and machinery. The main engine is a Wartsila 16V26D2 and the auxiliary generator sets are MTU Motor 16V2000 M60. In Fig. 22 we can see the distribution of the nodes: Node 0 (master) in the most centered place of the deployment, in the adjacent compartment on a box close to the door at 1.5 m; nodes 1 and 2 on the floor at the opposite side of the adjacent room, while nodes 3 and 4 at 1.5 m elevation on top of metal boxes; nodes 5 and 6 on the floor one on each side of the door; one node on top of each generator set (7 and 8, although only the gen-

erator below node 8 was turned on); node 9 on the floor at the top corner of the engine room; node 10 on top of a metal box at 1.5 m; nodes 13 and 14 on top of the main engine, and nodes 11 and 15 at the bottom; Node 12 on top of the companion ladder to the upper deck; node 16 and 17 on each side of the gearbox attached to the engine.

Although the previous experiments in the engine room emulator did not show a notable effect of the machinery in the communications, since this engine is more powerful and the scenario more complex, we tested the communications with the machinery on/off (main engine, one generator set and pumping system). We combined this with the same three powers as in the previous scenario, adding also the door opening as a variable with the three opening levels we used in the freight containers, Table 8, to form a full factorial experiment of 6 runs per power. We completed the experiments on April 20th 2017, with the same configuration parameters as in the other environments.



(a) Transmission power at 0 dBm



(b) Transmission power at -10 dBm

Fig. 19 Number of dead ($PDR = 0\%$), poor ($PDR < 10\%$), intermediate ($10\% \leq PDR \leq 90\%$), good ($90\% < PDR < 100\%$), and perfect ($PDR = 100\%$) links for each node, for the engine room emulator environment.

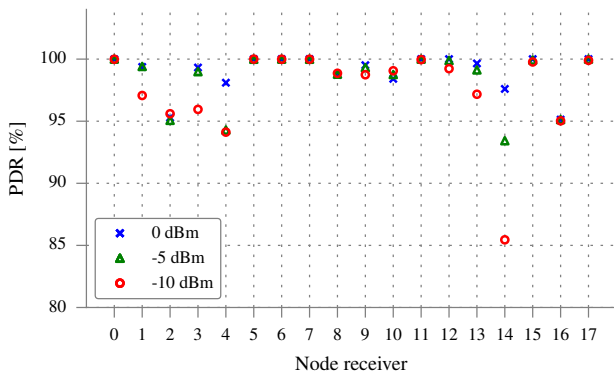


Fig. 20 Average total PDR [%] per individual node, for the engine room emulator environment.

6.2 Results & analysis

6.2.1 Overall network analysis

Since this environment is even more complex than the engine room emulator, we observe a larger number of outliers in the PDR and LQI vs RSSI measurements, shown in

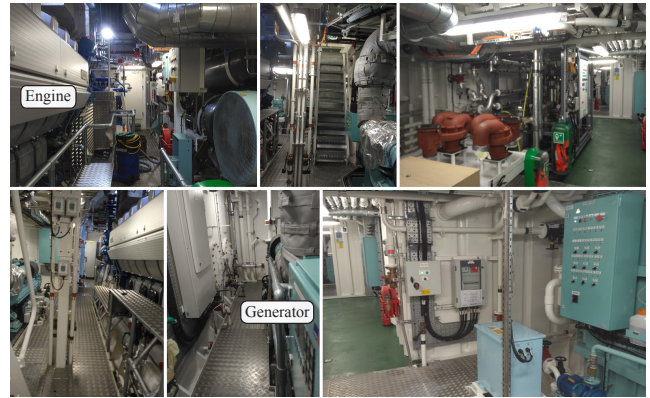


Fig. 21 Naval ship's engine room.

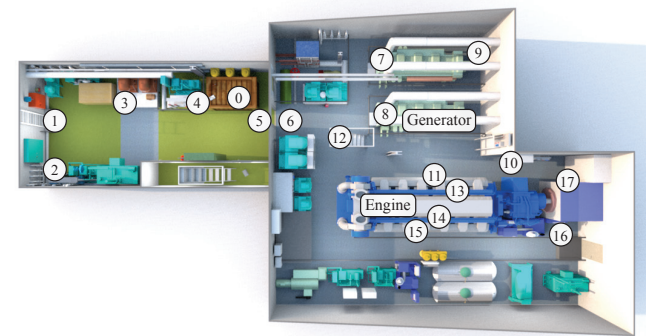


Fig. 22 Node distribution in the naval ship's engine room.

Table 8 Experiment variables.

Variable	Levels
Transmission power	0 dBm, -5 dBm, -10 dBm
Machinery status (main engine + generator)	on, off
Door opening	Closed, Open 5 cm, Open 40 cm

Fig. 23 and Fig. 24, such that the L-shape is no longer visible. We notice that an extra transition band is formed around -60 dBm for all power configurations, showing that even with a very high average signal strength and packet delivery ($RSSI = -62$ dBm, $PDR = 91.87\%$) the communications are very unpredictable. This is confirmed in the 3D plots in Fig. 25, where, despite having a large number of the probes in the 100% plane, a cloud of probes appears randomly distributed across the rest of the space. As expected, the noise floor remained at -96 dBm average.

We can see further how the unreliability is increasing in this environment by looking at the asymmetry between links in Fig. 26, where it reaches up to 20% for nodes 12-15, although it is still below the 40% that defines a link as asymmetric.

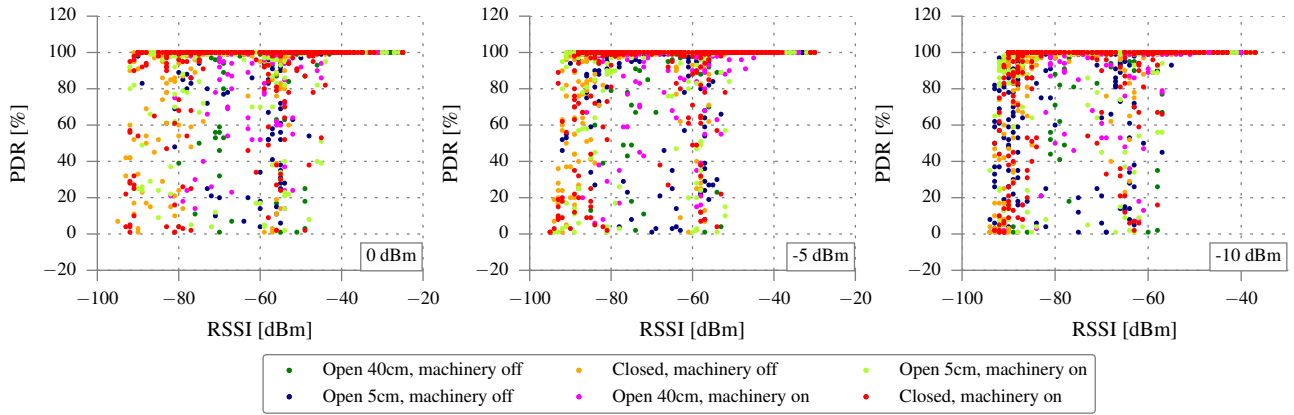


Fig. 23 PDR vs RSSI for the naval ship's engine room environment.

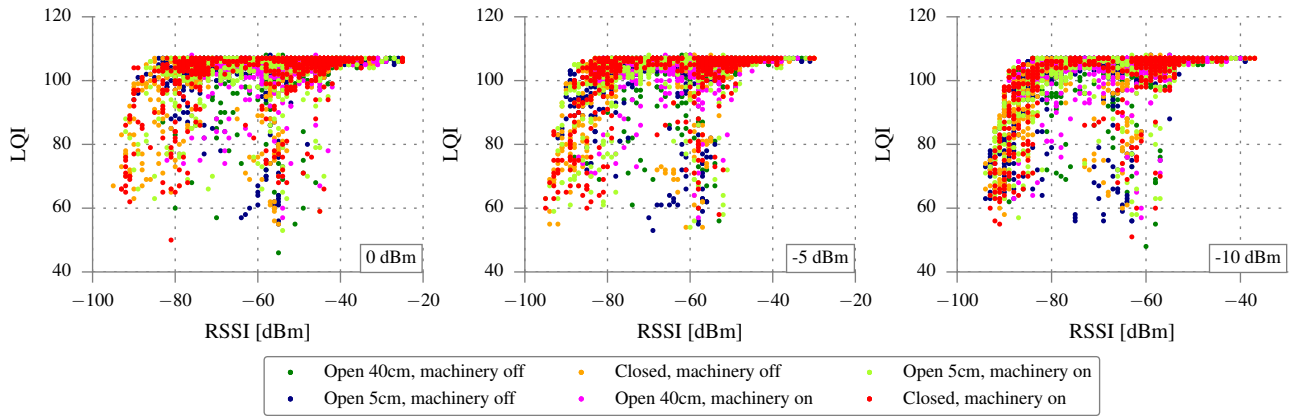


Fig. 24 LQI vs RSSI for the naval ship's engine room environment.

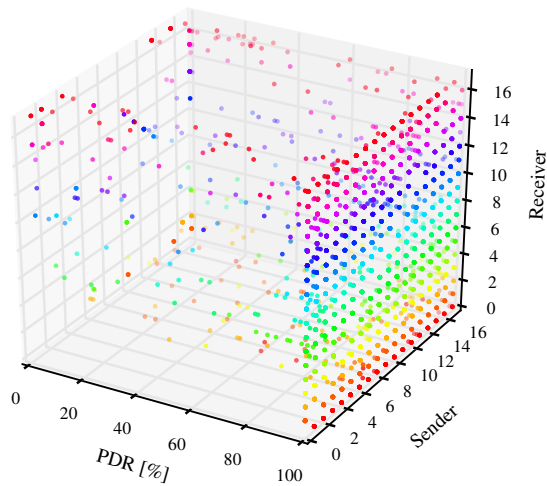
6.2.2 Effects of the variables on network performance

To explore the effect the machinery has on the communications, we show in Table 9 the average PDR and RSSI per power with the machines on/off. As we observed in the engine room scenario, although we can also see here a small drop in PDR, it does not have an important effect. Even for the low power configuration (-10 dBm) we have a decrease only from 89.09% to 88.93%. This effect is confirmed by looking at the CDF of the PDR (Fig. 27) and more clearly the RSSI (Fig. 28), where we can see that each pair of lines corresponding to the machines on/off for each door configuration run together following the same shape. A greater impact is produced by the door opening (Table 10), as we reported in the freight containers environment. Despite the door being waterproof sealed when closed, we only see a reduction from 88.76% at 5 cm opening to 81.29% when closed, at -10 dBm transmission power.

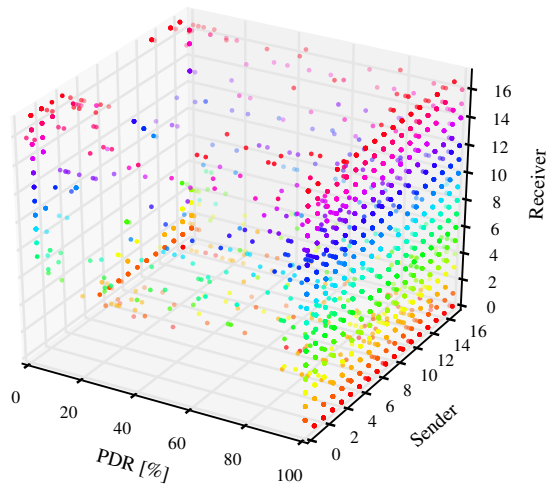
The average temperature was kept constant by the AC system at 24.85 °C, with a $\sigma = 4.63$, again due to the increase in the surface temperature of the machines measured by the nodes placed on them.

6.2.3 Link classification and sink selection

While the PDR vs RSSI and 3D plots suggested an unstable network, the average links per node all show above 10% PDR connectivity for high and low power, as we see in Fig. 29. However, for the worst case rounds where the machines are on and the door closed (Fig. 30), we observe dead links in all the nodes that are farther from the sliding door. Nodes 0, 4, 5, 6, 7 and 8 present no dead links, which makes them good sink candidates. Although node 12 is also close to the door, it performs worse due to being placed on top of the companion ladder with no line of sight. In Fig. 31 we see that node 6, located next to the door in the engine room, presents the highest overall PDR, with around 97% for the three power configurations, while nodes 1, 2 and 17 (located at the end of each room) have the lowest with around 75% for the low power configuration. This suggests that whenever we have sealed doors that could be closed, we need to have a sink or node with forwarding capabilities near the door.



(a) Transmission power at 0 dBm



(b) Transmission power at -10 dBm

Fig. 25 PDR [%] between each node for all rounds at different transmission powers, for the naval ship's engine room environment.

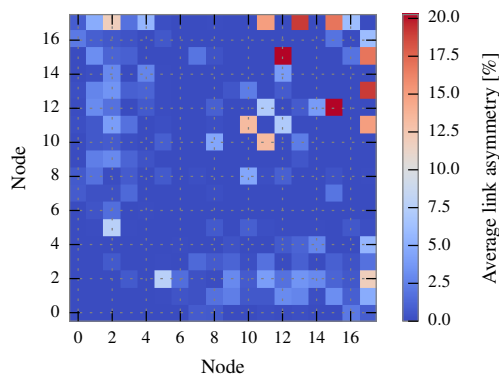


Fig. 26 Link asymmetry calculated as $|PDR_{n \rightarrow m} - PDR_{m \rightarrow n}|$, for the naval ship's engine room environment.

Table 9 Average PDR and RSSI for different machinery states.

Transmission power	Machinery state	PDR [%]	RSSI [dBm]
0 dBm	Off	94.02	-58
	On	94.17	-57
-5 dBm	Off	92.75	-62
	On	92.25	-62
-10 dBm	Off	89.09	-67
	On	88.93	-67

Table 10 Average PDR and RSSI for different door openings.

Transmission power	Door state	PDR [%]	RSSI [dBm]
0 dBm	Closed	91.28	-61
	Open 5 cm	94.38	-58
	Open 40 cm	96.64	-54
-5 dBm	Closed	87.43	-65
	Open 5 cm	93.20	-63
	Open 40 cm	96.87	-59
-10 dBm	Closed	81.29	-69
	Open 5 cm	88.76	-68
	Open 40 cm	96.98	-64

7 Conclusions & Future work

In this paper, we studied through experimentation the physical link quality of a wireless sensor network in three different metallic scenarios. The first comprised three freight containers, creating an indoors-outdoors, multi-chamber metal environment, where we conducted a measurement campaign using 18 nodes in a randomized structured experiment, accounting for the effects of node position and orientation, door openings, and transmission power. The second was a large engine room emulator containing a ship's engine, several generators and large amounts of metal piping and gantries, where we tested the effects of the machinery running. The final set of experiments were in a naval vessel engine room and its adjacent compartment, accounting for the opening and closing of the waterproof door between them as well as the switching of the machinery. We recorded and analyzed the PDR, RSSI, and LQI for all the possible links in the network, and extracted an overview of the network behaviour as well as individual node performance.

From the results of the first scenario, we observe that the best case is obtained when transmitting at high power with the doors fully open and nodes horizontal at 1.7 m, with a PDR = 74.69%, while the worst case is found at low power, doors closed and nodes vertical at ground level, yielding a

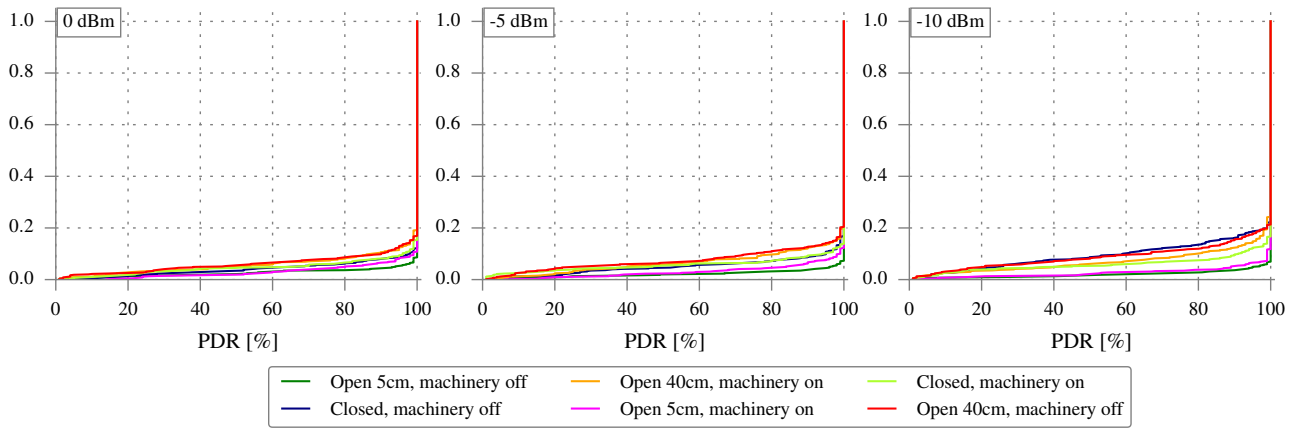


Fig. 27 CDF of the PDR for the naval ship's engine room environment.

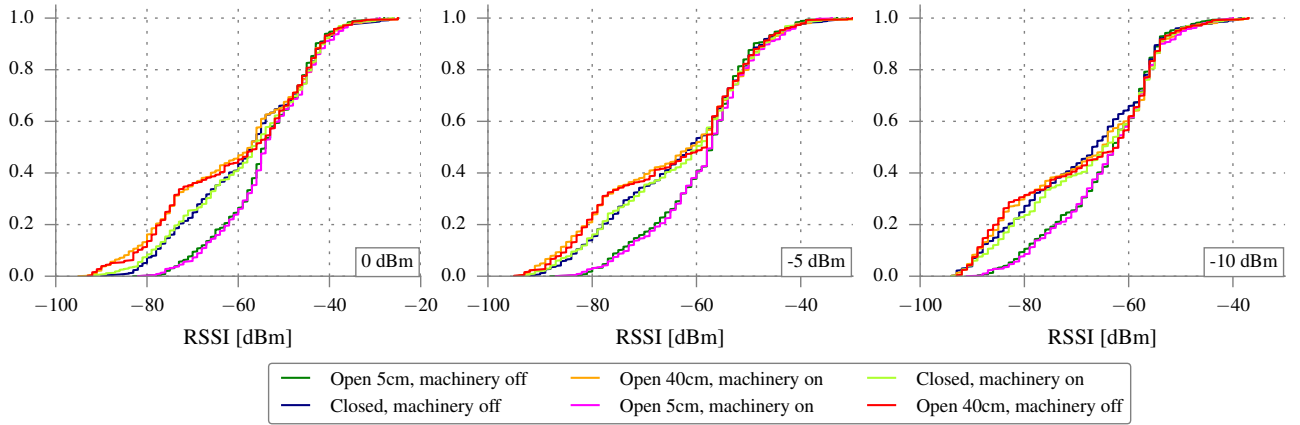
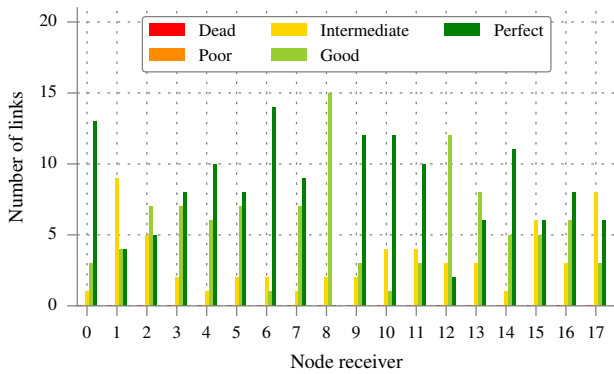


Fig. 28 CDF of the RSSI for the naval ship's engine room environment.

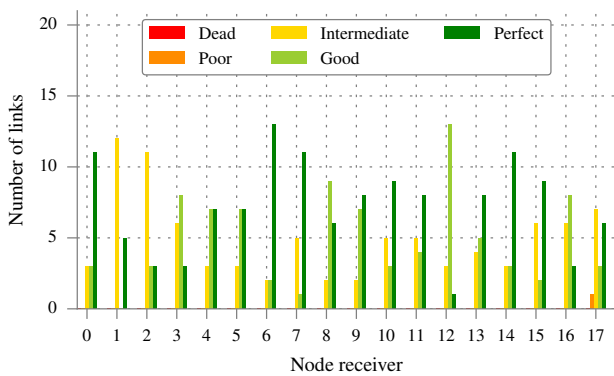
PDR = 37.25%. We identify the door openings as the variable having the most impact on the overall network performance. The best sink candidate was selected, with an average PDR = 91.97% from the remaining nodes at a high transmission power (0 dBm), a PDR = 80.65% for the closed doors, and a PDR = 96.92% with just a 5 cm opening. This suggested that a wireless sensor network could be a feasible low-cost alternative to wired sensors under various conditions in metallic environments. However, when we analyze the results of the second scenario we see that although the overall network performance is very high (PDR = 98.32%), the increasing complexity of the environment, i.e. more extensive volume occupancy of metal and machinery, yields a wider transition zone, making the communications more unpredictable. This was especially noticeable in the nodes attached to the engine, where the one placed inside the metal cover unexpectedly performed much better than the one on top. The final experiments, performed in the naval vessel engine room, confirmed that the more complex the scenario, the more unreliable the communications. Although the results in the naval still showed a high PDR, with PDR = 80.65%

even with the door fully closed and transmitting at -10 dBm, the transition zone in this environment is much wider occupying most of the area as we can see in the PDR vs RSSI plots. From this we can conclude that even if a path-loss model based on distance and RSSI were developed for those scenarios, it would not have any meaningful capabilities of predicting the PDR of each node. Therefore, to deploy a WSN in these environments a systematic practical study must be done on each specific target scenario, including a connectivity assessment similar to the one demonstrated in this paper, to identify areas of difficult connectivity and optimal sink location.

By focusing on low-level physical network analysis in real scenarios, we achieve a more accurate characterization of the environment, in contrast with the higher-layers studied in prior works. We believe that the methodology, verified in the three scenarios, we have presented in this paper is both straightforward and practical for WSN planning in general metallic environments both marine and also land-based e.g. in typical manufacturing environments with large amounts of piping, ducting and machinery.



(a) Transmission power at 0 dBm



(b) Transmission power at -10 dBm

Fig. 29 Number of *dead* ($PDR = 0\%$), *poor* ($PDR < 10\%$), *intermediate* ($10\% \leq PDR \leq 90\%$), *good* ($90\% < PDR < 100\%$), and *perfect* ($PDR = 100\%$) links for each node, for the naval ship’s engine room environment.

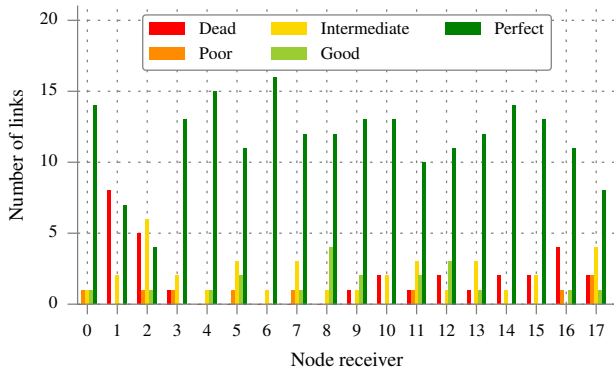


Fig. 30 Link classification for the closed door and machinery on round, at -10 dBm.

The information obtained using this methodology can be used to deploy real sensor network applications in these and similar scenarios. This data can be used with the method described in [28] to mitigate multi-path fading either repositioning the nodes or using channel hopping techniques, similar to the ones used also in the industrial standard for WSN

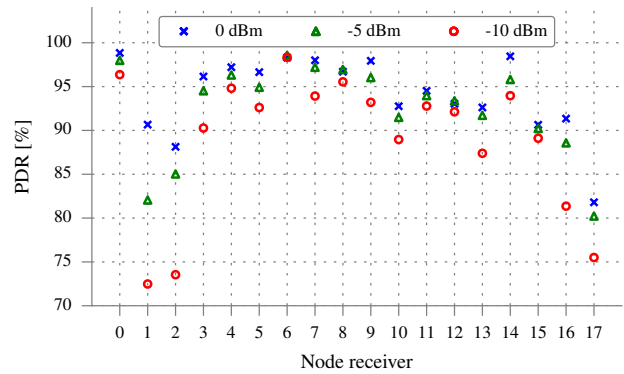


Fig. 31 Average total PDR [%] per individual node, for the naval ship’s engine room environment.

WirelessHART [8]. For nodes close to heavy machinery that can reach high temperatures, the technique used in [5] can improve the reliability by dynamically adapting the CCA threshold at runtime depending on the temperature measured locally on the node. The CCA adjustment will also be useful if a high noise floor is detected in some particular locations, as demonstrated in [16], where a deployment in a data center was shown to be failing due to some nodes not sending packets due to having a noise floor higher than the configured CCA threshold. With these techniques combined, as well as the methodology described in this paper, a more robust WSN deployment can be achieved with the reliability required for this type of scenarios.

Acknowledgements The authors would like to thank Conor Mowlds, Vivian Gough, Paul Nash and Tim P. Forde from the National Maritime College of Ireland (NMCI), as well as Commodore Hugh Tully, Lieutenant Commander David Memery and Lieutenant (NS) Padraig Reaney from the Irish Naval Service (INS), for their valuable help and support during the data collection for this paper and the overall project.

References

1. Alemdar H, Ersoy C (2010) Wireless sensor networks for healthcare: A survey. *Computer Networks* 54(15):2688–2710
2. Aygün B, Cagri Gungor V (2011) Wireless sensor networks for structure health monitoring: recent advances and future research directions. *Sensor Review* 31(3):261–276
3. Baccour N, Koubâa A, Mottola L, Zúñiga MA, Youssef H, Boano CA, Alves M (2012) Radio link quality estimation in wireless sensor networks: a survey. *ACM Transactions on Sensor Networks (TOSN)* 8(4):34
4. Bertocco M, Gamba G, Sona A (2008) Assessment of out-of-channel interference effects on IEEE 802.15.4 wireless sensor networks. In: *Instrumentation and Mea-*

- surement Technology Conference Proceedings, 2008. IMTC 2008. IEEE, IEEE, pp 1712–1717
5. Boano CA, Römer K, Tsiftes N (2014) Mitigating the adverse effects of temperature on low-power wireless protocols. In: Mobile Ad Hoc and Sensor Systems (MASS), 2014 IEEE 11th International Conference on, IEEE, pp 336–344
 6. Ceriotti M, Chini M, Murphy AL, Picco GP, Cagnacci F, Tolhurst B (2010) Motes in the jungle: lessons learned from a short-term wsn deployment in the ecuador cloud forest. In: Real-World Wireless Sensor Networks, Springer, pp 25–36
 7. Ferens K, Woo L, Kinsner W (2009) Performance of zigbee networks in the presence of broadband electromagnetic noise. In: Electrical and Computer Engineering, 2009. CCECE'09. Canadian Conference on, IEEE, pp 407–410
 8. Foundation HC (2006) Hart field communication protocol specification. HFC_SPEC12, Revision 6
 9. Ganesan D, Krishnamachari B, Woo A, Culler D, Estrin D, Wicker S (2002) Complex behavior at scale: An experimental study of low-power wireless sensor networks. Tech. rep., Citeseer
 10. Istomin T, Marfievici R, Murphy AL, Picco GP (2014) Trident: In-field connectivity assessment for wireless sensor networks. In: Proceedings of the 6th Extreme Conference on Communication and Computing (ExtremeCom)
 11. Kdouh H, Zaharia G, Brousseau C, El Zein G, Grunfelder G (2011) Zigbee-based sensor network for shipboard environments. In: Signals, Circuits and Systems (ISSCS), 2011 10th International Symposium on, IEEE, pp 1–4
 12. Kdouh H, Brousseau C, Zaharia G, Grunfelder G, Zein G (2012) A realistic experiment of a wireless sensor network on board a vessel. In: Communications (COMM), 2012 9th International Conference on, IEEE, pp 189–192
 13. Kdouh H, Farhat H, Zaharia G, Brousseau C, Grunfelder G, Zein G (2012) Performance analysis of a hierarchical shipboard wireless sensor network. In: Personal Indoor and Mobile Radio Communications (PIMRC), 2012 IEEE 23rd International Symposium on, IEEE, pp 765–770
 14. Kdouh H, Zaharia G, Brousseau C, Grunfelder G, Farhat H, El Zein G (2012) Wireless sensor network on board vessels. In: Telecommunications (ICT), 2012 19th International Conference on, IEEE, pp 1–6
 15. Marfievici R, Murphy A, Picco G, Ossi F, Cagnacci F (2013) How environmental factors impact outdoor wireless sensor networks: A case study. In: Mobile Ad-Hoc and Sensor Systems (MASS), 2013 IEEE 10th International Conference on, pp 565–573, DOI 10.1109/MASS.2013.13
 16. Marfievici R, Corbalán P, Rojas D, McGibney A, Rea S, Pesch D (2017) Tales from the c130 horror room: A wireless sensor network story in a data center. In: Proceedings of the First ACM International Workshop on the Engineering of Reliable, Robust, and Secure Embedded Wireless Sensing Systems, ACM, New York, NY, USA, FAILSAFE'17, pp 24–31
 17. Ovsthus K, Kristensen LM, et al (2014) An industrial perspective on wireless sensor networks: a survey of requirements, protocols, and challenges. IEEE Communications Surveys & Tutorials 16(3):1391–1412
 18. Pilsak T, ter Haseborg JL (2010) Simulation of wireless sensor networks on vessels under consideration of emc. In: Electromagnetic Compatibility (APEMC), 2010 Asia-Pacific Symposium on, IEEE, pp 602–605
 19. Polastre J, Szewczyk R, Culler D (2005) Telos: enabling ultra-low power wireless research. In: Information Processing in Sensor Networks, 2005. IPSN 2005. Fourth International Symposium on, IEEE, pp 364–369
 20. Rashid B, Rehmani MH (2016) Applications of wireless sensor networks for urban areas: A survey. Journal of Network and Computer Applications 60:192–219
 21. Rehmani MH, Rachedi A, Lohier S, Alves T, Pousot B (2014) Intelligent antenna selection decision in iee 802.15. 4 wireless sensor networks: An experimental analysis. Computers & Electrical Engineering 40(2):443–455
 22. Rojas D, Barrett J (2016) Experimental analysis of a wireless sensor network in a multi-chamber metal environment. In: European Wireless 2016; 22th European Wireless Conference; Proceedings of, VDE, pp 1–6
 23. Rojas D, Barrett J (2017) A hardware-software wsn platform for machine and structural monitoring. In: Signals and Systems Conference (ISSC), 2017 28th Irish, IEEE, pp 1–6
 24. Rondinone M, Ansari J, Riihijärvi J, Mähönen P (2008) Designing a reliable and stable link quality metric for wireless sensor networks. In: Proceedings of the workshop on Real-world wireless sensor networks, ACM, pp 6–10
 25. Sexton D, Mahony M, Lapinski M, Werb J (2005) Radio channel quality in industrial wireless sensor networks. In: Sensors for Industry Conference, 2005, IEEE, pp 88–94
 26. Srinivasan K, Dutta P, Tavakoli A, Levis P (2010) An empirical study of low-power wireless. ACM Transactions on Sensor Networks (TOSN) 6(2):16
 27. Suryadevara NK, Mukhopadhyay SC, Kelly SDT, Gill SPS (2015) Wsn-based smart sensors and actuator for power management in intelligent buildings. IEEE/ASME transactions on mechatronics 20(2):564–571

28. Watteyne T, Lanzisera S, Mehta A, Pister KS (2010) Mitigating multipath fading through channel hopping in wireless sensor networks. In: Communications (ICC), 2010 IEEE International Conference on, IEEE, pp 1–5
29. Xu G, Shen W, Wang X (2014) Applications of wireless sensor networks in marine environment monitoring: A survey. *Sensors* 14(9):16,932–16,954
30. Yeoh CM, Chai BL, Lim H, Kwon TH, Yi KO, Kim TH, Lee CS, Kwark GH (2011) Ubiquitous containerized cargo monitoring system development based on wireless sensor network technology. *International Journal of Computers Communications & Control* 6(4):779–793
31. Yu X, Wu P, Han W, Zhang Z (2013) A survey on wireless sensor network infrastructure for agriculture. *Computer Standards & Interfaces* 35(1):59–64
32. Yuan S, Becker M, Jedermann R, Görg C, Lang W (2009) An experimental study of signal propagation and network performance in monitoring of food transportation. In: Sensor, Mesh and Ad Hoc Communications and Networks Workshops, 2009. SECON Workshops' 09. 6th Annual IEEE Communications Society Conference on, IEEE, pp 1–3
33. Zhao J, Govindan R (2003) Understanding packet delivery performance in dense wireless sensor networks. In: Proceedings of the 1st international conference on Embedded networked sensor systems, ACM, pp 1–13
34. Zinonos Z, Vassiliou V, Christofides T (2012) Radio propagation in industrial wireless sensor network environments: From testbed to simulation evaluation. In: Proceedings of the 7th ACM workshop on Performance monitoring and measurement of heterogeneous wireless and wired networks, ACM, pp 125–132



David Rojas is currently pursuing the Ph.D. degree in electronics engineering with the Nimbus Centre for Embedded Systems Research, Cork Institute of Technology, Cork, Ireland. He is involved in the development of different wireless modules for structure and machine monitoring, as well as characterizing wireless sensor network communications

in marine harsh environments. His current research interests include embedded systems, wireless sensor networks and packaging solutions for electronic sensor devices.



John Barrett was an Assistant Director of the Tyndall National Institute, University College Cork, Cork, Ireland. He joined the Cork Institute of Technology, Cork, Ireland, in 1999, as a Lecturer, where he is currently the Head of Academic Studies with the Nimbus Centre for Embedded Systems Research. His research is focused on packaging, miniaturization, and embedding of smart systems in materials, objects, and structures with a particular emphasis on challenging and harsh application environments.

and structures with a particular emphasis on challenging and harsh application environments.